Article:
Davies, K, Afrough, B, Mankouri, J et al. (2019) Tula orthohantavirus nucleocapsid protein is cleaved in infected cells and may sequester activated caspase-3 during persistent infection to suppress apoptosis. Journal of General Virology, 100 (8). pp. 1208-1221. ISSN: 0022-1317

https://doi.org/10.1099/jgv.0.001291

Tula orthohantavirus nucleocapsid protein is cleaved in infected cells and may sequester activated caspase-3 during persistent infection to suppress apoptosis

Katherine Davies[1], Babak Afrough[2], Jamel Mankouri[1, 3], Roger Hewson[2], Thomas A. Edwards[1, 3], John N. Barr[1, 3†]

[1]School of Molecular and Cellular Biology, University of Leeds, Leeds, LS2 9JT, UK
[2]National Infection Service, Public Health England, Porton Down, Salisbury SP4 0JG, UK
[3]Astbury Centre for Structural Molecular Biology, University of Leeds, Leeds, LS2 9JT, UK

Running title: TULV NP sequesters cleaved caspase-3

Word Count: Abstract: 247; Main text (excluding references) 5564.

Keywords: Apoptosis, Tula virus, Orthohantavirus, Caspase, Nucleocapsid Protein, Persistence

†To whom correspondence should be addressed Tel: +44 (0)113-3438069; E-mail: j.n.barr@leeds.ac.uk

ABSTRACT

The *Hantaviridae* family comprises mostly rodent-borne segmented negative sense RNA viruses, many of which are capable of causing devastating disease in humans. In contrast, hantavirus infection of rodent hosts results in a persistent and inapparent infection through their ability to evade immune detection and inhibit apoptosis. In this study, we used Tula hantavirus (TULV) to investigate the interplay between viral and host apoptotic responses during early, peak and persistent phases of virus infection in cell culture. Examination of early phase TULV infection revealed that infected cells were refractory to apoptosis evidenced by the complete lack of cleaved caspase-3 (casp-3C) staining, whereas in non-infected bystander cells casp-3C was highly abundant. Interestingly at later time points, casp-3C was abundant in infected cells, but cells remained viable and able to continue shedding infectious virus, and together these observations were suggestive of a TULV-associated apoptotic block. To investigate this block, we viewed TULV-infected cells using laser scanning confocal and wide-field deconvolution microscopy, which revealed TULV nucleocapsid protein (NP) colocalized with, and sequestered, casp-3C within cytoplasmic ultrastructures. Consistent with casp-3C colocalization, we showed for the first time that TULV NP was cleaved in cells and that TULV NP and casp-3C could be co-immunoprecipitated, suggesting this interaction was stable and thus unlikely solely confined to NP binding as a substrate to the casp-3C active site. To account for these findings, we propose a novel mechanism by which TULV NP inhibits apoptosis by spatially sequestering casp-3C from its downstream apoptotic targets within the cytosol.

INTRODUCTION

The *Orthohantavirus* genus within the *Hantaviridae* family comprises many zoonotic segmented negative sense (SNS) RNA viruses that are capable of causing devastating human disease, often with fatal outcomes. Orthohantaviruses are broadly-spherical enveloped viruses, which possess a tripartite genome made up of small (S), medium (M) and large (L) RNA segments that minimally-encode the nucleocapsid protein (NP), glycoprotein precursor (GPC) and RNA dependent RNA polymerase (RdRp), respectively [1, 2]. Many members of the family also encode a small non-structural protein (NSs) accessed from an alternate open reading frame, and which acts as an antagonist of the innate immune response [3–5].

Orthohantaviruses can be divided into New World (NW) and Old World (OW) clades based on their country of isolation, with OW viruses being widespread throughout Asia and Europe, and NW viruses found in the Americas [6]. Orthohantaviruses are typically associated with a specific rodent host, although recent evidence suggests that bats, shrews, moles and ray-finned fish also act as reservoirs [7, 8]. Orthohantaviruses have been shown to cause persistent, often apathogenic infections in these hosts, although there is some evidence to suggest infection is associated with reduced host survival [9–13] with histological examination of lungs, heart and livers of infected animals showing some signs of pathology [14].

Orthohantaviruses are transmitted to humans by the inhalation of aerosolised excreta and other body fluids from the infected animal host, although direct human-to-human transmission has also been reported for Andes virus (ANDV) [15]. Several human pathologies have been observed for different orthohantavirus species, with the disease outcome closely correlating with the two orthohantavirus clades; OW orthohantaviruses are associated with haemorrhagic fever with renal syndrome (HFRS), whilst NW orthohantaviruses are the causative agent of hantavirus cardiopulmonary syndrome (HCPS). While these syndromes afflict different primary organs, both are characterised by excessive vascular leakage leading to shock, with human mortality rates ranging from 0.1-10% for HFRS and up to 40% for HCPS [16, 17]. Endothelial cells are the primary sites of hantavirus multiplication, although these cells do not display overt cytopathic effects [18]. This outcome is recapitulated in cell culture systems in which orthohantavirus infections are not associated with excessive cytopathology or cell lysis, and instead infections can become persistent with on-going virus shedding for up to 139 days post infection in the case of Seoul virus (SEOV) [19–21]. The ability of hantaviruses to persist suggests they are able to evade pathogen surveillance, and avoid innate immune defence mechanisms such as apoptosis.

Apoptosis is an important component of cellular homeostasis. There are many apoptotic pathways, including the caspase cascade in which a series of cysteine-aspartate proteases are activated by cleavage [22]. Viruses have developed complex mechanisms to

97 modulate apoptotic signalling pathways to benefit their own survival, which can result in either
98 delay or acceleration of apoptosis with pro-viral outcomes.
99 There is considerable evidence to suggest that hantaviruses prevent the induction of
100 apoptosis, consistent with their ability to establish persistence. Puumala virus (PUUV) NP has
101 been shown to interact with the Fas-mediated apoptosis enhancer Daxx [23], whilst NP from
102 Hantaan virus (HTNV) modulates apoptosis though down-regulating p53 [24]. Furthermore,
103 a panel of six hantaviruses spanning three distinct serogroups (ANDV, Dobrava virus (DOBV),
104 HTNV, PUUV, SEOV and Tula virus (TULV)) were each recently shown to supress apoptosis
105 in staurosporine-treated cells. The same study suggested that NP plays a direct role in
106 modulating apoptosis through the demonstration that NP can be cleaved by purified caspase-
107 3. In addition, recombinant N protein from ANDV, DOBV and PUUV have been shown to inhibit
108 both caspase-3 and granzyme B in cell free assays [25, 26].
109 To better characterise the role of the hantavirus NP in modulating apoptosis, we used
110 the model OW orthohantavirus TULV to examine how NP interacts with key components of
111 the apoptotic machinery through an extended time course spanning early, peak, and a
112 persistently-infected state. We demonstrate that TULV infection can persist for over 30 days
113 in mammalian cells, with little or no apoptosis induction desite abundant levels of cleaved
114 caspase 3 (casp-3C). We further show that TULV NP forms both punctate and tubular
115 ultrastructures within intermediate and persistently-infected cells, in which active casp-3C is
116 physically sequestered as a consequence of a robust and stable association with NP, leading
117 to NP cleavage. We thus propose a model in which the ability of TULV to suppress apoptosis
118 is driven by interactions between NP and casp-3C, leading to NP cleavage, and spatial
119 separation of the executioner caspase from its downstream effectors.
120

METHODS

Cell culture

TULV Moravia strain 5302v/95 and Vero E6 cells were kindly provided by Dr Roger Hewson, Public Health England, UK. Virus propagation was carried out in Vero E6 cells grown in Dulbecco's modified Eagle medium (DMEM) supplemented with 10% foetal bovine serum (FBS) (Sigma Aldrich), 100 U/mL penicillin and 100 µg/mL streptomycin at 37°C in a 5% CO_2 atmosphere. TULV stocks were confirmed as mycoplasma-free using MycoAlert™ (Lonza).

Nucleocapsid protein production and purification

A cDNA representing the NP open reading frame (ORF) from SEOV strain Humber (accession number JX879769.1) optimized for bacterial expression, was generated synthetically (GeneArt, Therrmo Fisher) and inserted in the pMK-RQ vector. This was subsequently used as the template for amplification of the NP 'core', comprising residues E111-G399 (NP_{core}) using the primer set 5'-TGTTGGATCCGAACCGACAG GTCAGACCGCAGATTG-3' and 5'-GGTGCTCGAGTTAACCCAGGTGAAAGTTATCCACG GC-3'. The amplified core region was then cloned into the pET28a (+) expression vector behind sequences for both the 6xHis affinity tag, and the SUMO tag for over expression in *Escherichia coli* BL21 DE3 Gold cells. Bacterial cultures were induced using 0.5 mM IPTG and then incubated overnight at 18°C in a 180-rpm shaking incubator. Bacterial pellets were collected by centrifugation at 4,000 xg for 20 minutes at 4°C before resuspension in ice-cold lysis buffer (500 mM NaCl, 20 mM Tris-HCl pH 8, 20 mM $MgCl_2$, 5 mM β-mercaptoethanol, 1 % Triton X-100, 1 mg/ml lysozyme (Sigma Aldrich), 1 pellet EDTA-free protease inhibitors (Roche), 1 U RNase, 1 U DNase) and sonicated. The insoluble fraction was pelleted by centrifugation at 20,000 xg for 1 hour at 4°C and soluble protein collected in the supernatant. The soluble fraction was then applied to a 5 ml HisTrap™ (GE Healthcare) column and washed with 5 column volumes of 25-100 mM imidazole wash buffers (500 mM NaCl, 20 mM Tris, 5 mM β-Me). Recombinant NP_{core} was eluted from the column using 10 column volumes of elution buffer (500 mM imidazole, 500 mM NaCl, 20 mM Tris, 5 mM β-mercaptoethanol). The 6xHis SUMO tag was removed by incubation with 1U/ml Ulp1 protease overnight at 4°C. The cleaved protein was diluted 1:10 in 20 mM elution buffer before being passed over a 5 ml HisTrap™ column to remove tag and protease. The collected flow-through was concentrated in a 10 kDa molecular weight cut-off concentrator (Amicon) to 0.5 mg/ml. Purity (>85%) of the resulting NP_{core} was determined by densitometry following SDS-PAGE and Coomassie staining.

157 **Antibodies**

158 TULV NP antibody was generated in sheep with 4x 200 mg inoculations of recombinant
159 purified NP_{core} (Alta Biosciences, UK). Serum was collected pre-inoculation and post-1, -2, -3,
160 -4 inoculations. Serum was centrifuged at 4,000xg for 20 minutes at 4°C to remove debris
161 before being stored at -20°C. Polyclonal antibodies against cleaved caspase-3, caspase-3
162 and cleaved PARP were purchased from New England Biolabs and monoclonal antibodies
163 against GAPDH were purchased from GeneTex.
164
165 **Quantitative reverse transcriptase-PCR**

166 Quantitative RT-PCR was carried out as previously described [27] with adaptations to
167 the GoTaq® 1-Step RT-qPCR System Protocol (Promega). TULV S segment RNA was
168 isolated from infected cell culture medium using viral RNA mini kit (Qiagen) and reverse
169 transcribed using the primers 5'-GCCTCTAGAATGAGCCAACTCAAAGAAATACAAGAGG-3'
170 and 5'-GCCCTCGAGTTAGATTTTTAGCGGTTCCTGGTTTG-3'. The S segment ORF was
171 sub-cloned into pCDNA3.1 (+) T7 expression vector and used as template for transcription S
172 segment RNA using the mMESSAGE mMACHINE™ T7 Transcription Kit (Thermo Fisher
173 Scientific) and purified using the RNeasy mini kit (Qiagen). RNA purity was assessed using
174 electrophoresis examination (Fig 2A) and concentration adjusted to 10^8, 10^6, 10^4 and 10^2
175 genomic copies per quantitative RT-PCR (qRT-PCR) reaction (5 µl). Genomic copies of
176 experimental samples were determined from the generated standard curve.
177
178 **Virus infections**

179 Vero E6 cells were seeded out at a density of $1x10^5$ cells per well for a 12-well plate or
180 $1x10^6$ cells per 25 cm^2 flask. TULV was adsorbed to monolayers at MOI 1-0.1 in DMEM for 90
181 minutes before DMEM supplemented with 2% FBS, 100 U/ml penicillin and 100 µg/ml
182 streptomycin (2% DMEM) was added. Persistent TULV infections were carried out in 25 cm^2
183 flasks and infected cells were seeded onto coverslips 24 hours before fixation. Cells were fixed
184 in 4% paraformaldehyde at 36 hours post infection (hpi), 7 days post infection (dpi) and 30 dpi
185 to demonstrate early, peak and persistent infections.
186
187 **TULV time course**

188 Vero E6 cells were seeded out at a density of $6x10^5$ cells per well of a 6-well plate and
189 infected with TULV at a MOI 0.1. At each time point, cells were scraped into the cell culture
190 medium and stored at -80°C. Cell cultures were clarified by centrifuging at 20,000 xg for 10
191 minutes at 4°C. RNA extractions were carried out on clarified cell culture supernatant using
192 viral RNA mini kit (Qiagen) and RNA quantified in duplicate using 1-step qRT-PCR. Infectious
193 TULV was titrated in triplicate using an immunofluorescence assay.

194

195 **Virus titration**

196 Vero E6 cells were seeded out at a density of $5x10^3$ cells per well of a 96-well plate or
197 at $6x10^5$ cells per well of a 6-well plate and incubated at 37°C in 5 % CO_2 incubator overnight.
198 TULV was diluted 10^{-1} to 10^{-5} at a 1:10 dilution in DMEM. Diluted virus was adsorbed to cell
199 monolayers alongside neat TULV in volumes of 100 µl (96-well) and 200 µl (6-well). TULV
200 was adsorbed for 90 minutes at 37°C on a rocking platform. Following adsorption, 100 µl 2 %
201 FBS DMEM was added to 96-well plate cells and incubated at 37°C for 72 hours in a 5 % CO_2
202 incubator. For 6-well plates, inoculum was removed and overlaid with 3 ml 2% agarose diluted
203 1:1 in 2% FBS DMEM was added to each well and incubated at 37°C for 7 days in a 5 % CO_2
204 incubator. A second overlay of 2 ml 2% agarose diluted 1:1 in 2 % FBS DMEM was added
205 containing 45.3 µg/ml neutral red (Sigma Aldrich) before incubating at 37°C in a 5 % CO_2
206 incubator for a further 3 days. Plaques were considered areas with reduced staining and
207 counted [28]. 96-well plate cells were fixed in ice-cold methanol and infected cells were
208 identified through indirect staining using the anti-NP_{core} antibody in conjunction with an Alexa
209 Fluor 488 secondary antibody (Thermo Fisher Scientific). The Incucyte Zoom instrument
210 (Essen Bioscience) using a 10x objective lens was used to image infected monolayers. The
211 Incucyte ZOOM software was used to calculate the number of infected cells per well by
212 extrapolating an average a value from three fluorescent images of each well. Infectivity was
213 quantified as immunofluorescent units per ml (IU/ml), which represented the number of
214 resulting infectious foci per ml of inoculum. Each sample was quantified in triplicate.

215

216 **Indirect immunofluorescence**

217 Infected monolayers on coverslips were permeabilised in ice-cold methanol and
218 incubated at -20°C for at least one hour before being washed in 1x PBS and blocked in 5 %
219 BSA in 1x PBS (produced in-house). Primary antibody staining was carried out in 1% BSA in
220 1x PBS using sheep anti-NP_{core} at 1:2,000 dilution and rabbit anti-cleaved caspase-3 (casp-
221 3C) antibody at 1:200 dilution. Incubations were carried out for 2 hours at room temperature,
222 then washed thoroughly in 1x PBS. Secondary antibody staining was carried out using Donkey
223 anti-sheep Alexa Fluor 488 and Donkey anti-rabbit Alexa Fluor 647 at a 1:1,000 dilution for 1
224 hour. DAPI staining was carried out by incubating with 300 mM DAPI 5 minutes at room
225 temperature. Coverslips were mounted onto slides using VECTASHIELD Antifade Mounting
226 Medium (Vector laboratories) and sealed using clear nail polish. Infected cells were imaged
227 using the Zeiss LSM880 Upright confocal microscope at 40x magnification (Carl Zeiss Ltd)
228 and the DeltaVision Widefield Deconvolution microscope at 100x magnification (GE
229 Healthcare).

230

Western blotting

TULV infections, as described above, were carried out on Vero E6 monolayers in 6-well plates. At 24, 48, 72, 96, 120, 144, 168, 192, 216 and 240 hpi cells were scraped into cell culture medium and collected by centrifugation at 20,000xg for 10 minutes at 4°C before resuspension in 50µl PBS. An equal volume of NuPage loading buffer (Thermo Fisher) was added and samples were heated at 95°C for 5 minutes. Protein samples were separated by 15% SDS-PAGE and then transferred to an Immobilon-FL Polyvinylidene difluoride (PVDF) Membrane (Merck Millipore), which was probed with sheep anti-NP_{core}, rabbit anti-cleaved caspase 3 (casp-3C), caspase 3 (casp 3) and cleaved PARP (PARP-C). Mouse anti-GAPDH antibody was used as a loading control. Protein was detected using IRDye® 800CW Donkey anti-Goat IgG (H + L), IRDye® 800CW Donkey anti-Rabbit IgG (H + L) and IRDye® 680RD Donkey anti-Mouse IgG (H + L) and visualised by the Odyssey Imaging system (LI-COR). Densitometry was carried out using Fiji software.

Co-immunoprecipitation

Three 175cm^3 flasks of Vero E6 cells at 60% confluency were infected with TULV at a MOI of 0.1, as previously described. At 30 dpi cells were scraped into the cell culture medium and centrifuged at 4,000 xg for 10 minutes at 4°C. Supernatant was discarded and the cell pellet was washed in 1x PBS, followed by resuspension in ice-cold lysis buffer (150mM NaCl, 50mM TrisHCl (pH 8.0) 1% NP-40 alternative, 0.1% sodium dodecyl sulphate, 1x EDTA free protease inhibitor tablets (Roche)) and incubated on ice for 30 minutes before clarified by centrifuging at 1,000 xg for 10 minutes. Clarified lysate was used for TULV NP immunoprecipitation with anti-NP_{core} using Dynabeads™ Protein G Immunoprecipitation Kit (Thermo Fisher Scientific) following the manufacturers instructions. 1x NuPAGE loading dye was added directly to beads and samples were heated at 95°C for 5 minutes. Samples were centrifuged at 10,000 xg to pellet beads and supernantant was added to SDS-PAGE gels. Mock samples were treated similarly to infected, but without addition of TULV.

RESULTS

Generation of tools to quantify TULV components and infectivity. To characterise the progression of TULV infection in cells throughout an extended time course, we first developed tools to accurately quantify both TULV components and infectivity. For TULV protein detection, we generated NP antisera, and based on phylogenetic analysis of OW clade hantavirus NP amino acid sequences, we selected the SEOV NP to raise polyclonal antisera that would be broadly cross-reactive to multiple hantavirus NPs, including TULV. The SEOV NP core (residues 111-399; NP_{core}) was bacterially-expressed and purified (Fig 1a, left panel) and used for antibody production. The resulting antisera showed cross-reactivity against recombinant SEOV NP_{core} expressed in bacteria by western blot analysis (Fig 1a, right panel) and against TULV NP generated in TULV-infected cells at 6 days post-infection (dpi) assessed by both western blotting (Fig 1b) and immunofluorescence (Fig 1c). These results confirmed the high specificity of the antisera, as evidenced by absent background or non-specific staining in mock-infected cells. In agreement with previous studies, TULV NP was detected in perinuclear ultrastructures, and cytoplasmic puncta [20].

Alongside the production of NP antisera, we also established a rapid PCR-based assay for the quantitative detection of TULV vRNA replication products, calibrated using a standard curve generated using *in vitro* transcribed TULV S segment vRNA at a range of concentrations. The purity of the vRNA was verified using electrophoresis (Fig 1d) and Rsq values ≥ 0.99 (Fig 1e).

Finally, we developed assays to measure TULV infection kinetics and virus production. Conventional infectivity assays reliant on plaque formation are problematical due to the low cytopathology of hantaviruses, with hantavirus infectivity often measured by neutral red uptake, which is both time-consuming and inaccurate, taking 10 days to produce poorly-visible plaques (Fig 2a). To remedy this, we developed an immunofluorescence (IF) based assay that relies on TULV NP antisera for detection of infected cells (Fig 2b). This method was used to examine the infectivity of a TULV dilution series and infected cell numbers followed a linear curve with a Rsq values ≥ 0.99 (Fig 2c).

Quantification of TULV components and infectivity across a 30-day time course. We next examined TULV multiplication and infectious particle production in Vero E6 cells over an extended time course. Cells were infected at an MOI of 0.1 after which supernatants and cell lysates were collected at regular timepoints up to 10 days post infection (dpi), with infections carried out at both 32 and 37°C. Additional samples from cultures incubated at 37°C were also taken at 15, 20, 25 and 30 dpi.

NP antisera was used to measure NP accumulation in cell lysates harvested from 37°C cultures by western blotting, which served as a marker for viral gene expression and virus

296 growth. Amplification of intracellular NP was first detected at 1 dpi (Fig 3a; 24 hpi), indicating
297 a significant lag prior to the onset of detectable gene expression, also reflecting the low MOI
298 used. Following this, NP abundance increased until 3 dpi (Fig 3a; 72 hpi), at which time NP
299 abundance reached a plateau that did not decline up to 10 dpi (Fig 3a; 240 hpi). NP abundance
300 relative to GAPDH was calculated using densitometry and represented graphically alongside
301 (Fig 3a).
302 Concomitantly, we used qRT-PCR to quantify the abundance of viral S segment RNAs,
303 harvested as virion-associated RNA within released virus particles in the supernatant. This
304 revealed a complex pattern that comprised an initial lag phase up to 30 hpi where viral RNA
305 levels showed no increase over input, indicating an initial lag in genome production and virus
306 release. This was subsequently followed by an exponential phase of rapid genome production,
307 and a plateau in RNA detection that extended to 10 dpi. This pattern of RNA detection was
308 observed in TULV grown at both 32°C and 37°C (Fig 3b) and was consistent with the profile
309 of NP detection shown above (Fig 3a). At later time points (15-30 dpi) genome abundance did
310 not increase further and gradually declined until the final 30 dpi measurement, although the
311 vRNA abundance remained at least 1 log higher than the initial input (Fig 3c).
312 To confirm that the detected RNA levels were due to the release of infectious virus
313 particles, and not the release of defective or fragmented RNAs, we also measured TULV
314 infectivity in the supernatants (Fig 3d and e). The overall pattern of infectivity closely followed
315 that of genome RNA abundance with the release of infectious virus remaining at a consistent
316 level until the 30 dpi harvest, a hallmark of a persistent infection. Based on these observations,
317 we defined 1.5, 7 and 30 dpi as the time points representing distinct early, peak and persistent
318 phases of virus multiplication, respectively.
319 IF analysis of TULV infected cultures using NP antisera at 1.5, 7 and 30 dpi time points
320 correlated with the above metrics (Fig 3f). At 1.5 dpi, NP staining was punctate and
321 perinuclear, whereas at 7 and 30 dpi, the staining pattern noticeably changed with NP forming
322 tubular ultrastructures in addition to distinct puncta. There was little evidence of nuclear
323 fragmentation in infected cells at any of these time points, suggestive of a lack of virus induced
324 apoptosis, although multinucleate syncytia were observed in the 30 dpi cultures.
325
326 **TULV infection interferes with apoptotic induction in Vero E6 cells**. The results
327 thus far showed that cultures of TULV-infected Vero E6 cells can be maintained for up to 30
328 dpi without major cytopathic effects. This suggests that TULV infection does not readily lead
329 to cell death, correlating with previous work that demonstrated the ability of hantaviruses to
330 subvert apoptotic induction. To further examine the apoptotic response of Vero E6 cells to
331 TULV infection, infected cell lysates were collected every 24 hours up to 10 dpi, and again at

30 dpi, and the levels of total caspase-3, cleaved caspase-3 (casp-3C), and cleaved poly (ADP-ribose) polymerase (PARP-C) assessed (Fig 4).

Total caspase-3 was detected in TULV-infected cells with its abundance increasing at later time points due to cell proliferation, consistent with the increasing abundance of the GAPDH loading control. The activated derivative casp-3C, indicative of apoptosis induction, was detected in TULV cell lysates from 5-6 dpi, with its abundance increasing up to 10 and 30 dpi. However, whilst this was suggestive of TULV induced apoptosis in infected cell cultures, a lack of PARP-C was evident at 6-10 dpi, and only moderate PARP-C cleavage was observed at 30 dpi. Furthermore, the high levels of casp-3C at 30 dpi were inconsistent with the apparent health of cells in these persistent cultures (Fig 3f). Taken together, these findings suggest that although the executioner casp-3C was present in its active form, it failed to trigger cell death in TULV infected cells, possibly due to the activity of a TULV component.

TULV induces apoptosis in bystander cells. The results thus far suggested that the downstream activity of executioner casp-3C may be suppressed in TULV-infected cells. We therefore investigated the intracellular location of casp-3C in relation to TULV NP in individual cells, first at at 1.5 dpi, representative of early stages of infection.

At 1.5 dpi, ~10% of cells were infected, as evidenced by characteristic punctate TULV NP staining, with numbers of infected cells correlating with the initial MOI of 0.1 (Fig 5a). In TULV-infected cells, NP staining was abundant, whilst minimal casp-3C was detected. Interestingly, casp-3C was abundant in uninfected bystander cells, with four such examples shown (Fig 5b), with casp-3C staining in a punctate distribution that extended throughout the cytoplasm suggesting apoptotic induction possibly through receiving indirect pathogen recognition signals from adjacent TULV-infected cells. We propose the likely fate of these cells is death. Casp-3C staining was detected in over 60% of bystander cells but only in 4% of TULV-infected cells (Fig 5c). Fluorescent line scan analysis (Fig 5b, right panel) quantified the expression of casp-3C in one such bystander cell, and revealed clear segregation from the TULV N stain in an adjacent infected cell (Fig 5d). These data suggest that during the early stages of virus infection, TULV is not a potent inducer of apoptosis, most likely through the ability of a TULV component to suppress apoptotic stimuli.

TULV NP sequesters casp-3C at later stages of infection. At 7 dpi, the majority of cells were infected by TULV, as evidenced by the accumulation of NP that exhibited both punctate staining, in addition to the formation of large tubular perinuclear structures (Figs 3f and 6a). These TULV-infected cells exhibited casp-3C staining, but it was noticeable that the levels of staining in relation to that exhibited within non-infected bystander cells was low, consistent with the suppression of apoptosis by a TULV component. Interestingly,

quantification of TULV NP and casp-3C staining by fluorescent line scan analysis revealed colocalization in several instances between the two markers within both characteristic puncta and larger tubular structures (Fig 6a; zoomed merge panel and associated line scan, left), although in other areas, the two signals were separate.

Examination of TULV persistently-infected cultures at 30 dpi revealed all cells to be TULV-infected, and exhibiting characteristic TULV NP staining within both discrete puncta and larger tubular structures. As at 7 dpi (Fig 6a), casp-3C was detected in these TULV-infected cells and fluorescent line scan analysis (Fig 6b, zoomed merge panel and associated line scan, left) revealed the colocalization of casp-3C with NP in both punctate and large tubular structures.

At these peak and persistent time points (7 and 30 dpi), when casp-3C was detected in TULV-infected cells, a distinct lack of apoptosis within the cells was evident, with most cells apparently healthy and able to sustain virus production (Fig 3e). These observations were difficult to reconcile with the abundance of casp-3C observed in these cells, other than a scenario in which active casp-3C was prevented from cleaving downstream substrates in the caspase cascade, possibly through its interaction with TULV NP.

Examination of TULV NP and casp-3C colocalization using widefield deconvolution microscopy. To further examine the colocalization of TULV NP and casp-3C in 30 dpi persistently-infected cells, infected cells were assessed by wide field deconvolution microscopy (WFDM) to enhance the detection sensitivity. As with confocal microscopy (Fig 6), WFDM also revealed that TULV-infected cells exhibited casp-3C staining within discrete cytoplasmic puncta (Fig 7a). While some areas of casp-3C staining were distinct from TULV NP, a high level of colocalization was observed, with the casp-3C staining appearing to be contained within that of TULV NP. Analysis of the spatial distribution of the two proteins using multiple fluorescent line scan analyses (Fig 7b; line scans below) confirmed and quantified the TULV NP and casp-3C colocalised signals, consistent with a scenario in which TULV NP compartmentalizes casp-3C. Quantification of TULV NP/casp-3C puncta abundance across early, peak and persistent TULV-cultures revealed an increased number of colocalized puncta through progression of the 30 day time course, with nearly 30% colocalization of the two proteins at 30 dpi (Fig 7b, histogram).

In other areas of persistently infected cells, NP and casp-3C staining remained separate, quantified using multiple line scans (Fig 7c), with quantitation of colocalization in early, peak and persistent TULV-cultures represented as a histogram.

TULV NP is cleaved in infected cells and robustly associates with casp-3C. For the orthohantavirus members ANDV, DOBV and PUUV, recombinant casp-3C has been

shown to mediate cleavage of their respective purified NPs in cell free assays [26]. In the case of ANDV, casp-3C cleaves ANDV NP at the sequence $DLID_{285}$, which conforms to the consensus DXXD motif for caspase-3 cleavage and generates a major NP fragment with molecular mass of approximately 35 kDa. With this knowledge combined with our observation that casp-3C and NP colocalize in TULV-infected cells, we next explored the possibility that TULV-NP acted as a cleavage substrate in infected cells.

Analysis of the TULV NP sequence revealed the presence of an identical DLID motif that is found in the ANDV NP, which was previously shown to be recongised and cleaved by casp-3C in cell-free assays. Interestingly, whilst the DLID motif was present in NPs from ANDV and TULV, it was absent in HTNV, PHV and SEOV (Fig 8a). Cleavage of the TULV NP at this site was predicted to generate TULV NP fragments of ~32 kDa and ~16 kDa. To test whether cleavage at this site occurs during infection, we examined TULV-infected cell lysates for NP-derived cleavage products by western blotting using anti-NP antisera, which revealed the abundant presence of NP cleavage products precisely matching these predicted masses (NP 32 kDa and NP 16 kDa, respectively; Fig 8b). The 16 kDa NP fragment was detected with high abundance at 3 dpi, which coincided with the initial detection of full-length NP, suggesting that NP cleavage occurs early during TULV infection. The fact that TULV NP possesses the same casp-3C target motif as ANDV, along with the consistent colocalization of TULV NP and casp-3C shown above, strongly implicates casp-3C as being responsible for the TULV NP cleavage we observed.

To further examine the TULV NP and casp-3C interaction, we next perfomed co-immunoprecipitation analysis using TULV NP antisera to pull down TULV NP and its interacting partners from 30 dpi TULV-infected cells. Subsequent western blot analysis of eluted fractions revealed the presence of full-length NP, as well as cleaved NP 32 kDa and NP 16 kDa forms, along with abundant casp-3C (Fig 8c). These data are entirely consistent with the co-localization studies described above (Fig 7b) and show the TULV NP and casp-3C interaction is highly stable. The ability of NP to pulldown casp-3C with such abundance argues for a scenario in which the interaction involves residues that are not confined to the casp-3C active site, which alone would be expected to result in an extremely transient enzyme:substrate interaction, not amenable to immunoprecipitation.

Taken together, we demonstrate for the first time that a hantaviral NP interacts with casp-3C in infected cells in a robust and stable manner, and we suggest the nature of this interaction results in physical sequenstration of casp-3C within NP compartments, and drives the suppression of the apoptotic response.

DISCUSSION

Here, we investigated the interplay between TULV and apoptosis induction in Vero E6 cells throughout an extended time course, spanning early, peak and persistent phases of infection. Previous work [23, 25, 26, 29] has shown that TULV and other hantaviruses inhibit apoptosis, and two observations made in our current study lend support to this proposal. First, while casp-3C was undetectable in TULV-infected cells at 1.5 dpi, in the same cultures, casp-3C was highly abundant in non-infected bystander cells, consistent with the ability of a TULV component to block apoptotic induction. Second, we showed that TULV can form persistently infected cultures up to 30 dpi without significant levels of CPE or the development of an apoptotic phenotype, despite casp-3C being highly abundant.

Our finding that TULV hinders apoptotic induction is in agreement with published work, but is in conflict with some previous studies in which TULV-infection was associated with abundant detection of apoptotic markers by western blotting [30–32]. However, we propose that this discrepancy may have arisen through technical differences in the approaches used to detect apoptotic markers. Here, we examined the spatial distribution of both NP and apoptotic markers in individual cells, rather than culture lysates that comprise both infected and uninfected cells. Whilst fluorescent imaging revealed the abundant detection of casp-3C at early time points following infection, it was predominantly located in bystander cells, rather than in TULV-infected cells. Thus, we propose that apoptosis of bystander cells, rather than TULV-infected cells, may be the source of apoptotic markers observed in previous studies. Bystander effects have been described previously in SEOV, HTNV, ANDV, [31] and HIV where the Env glycoprotein induces apoptotic induction in neighbouring cells [33] and has been utilised in cancer therapy by the use of “suicide genes” which allow production of a toxic metabolite that acts deleteriously on neighbouring cells [34].

Previous work has shown that a variety of hantaviral NPs, either expressed recombinantly, or purified from virions, can be cleaved in cell free assays by recombinant activated caspase 3. Here, we show that TULV NP is cleaved during infection (Fig 8a), with the apparent mass of released fragments being consistent with caspase-3 cleavage at a conserved DLID sequence, identical to that recently identified as a caspase-3 cleavage site for ANDV NP [26]. The role of TULV NP cleavage in these infected cells remains undetermined. One possibility is that it acts as a ‘decoy’ substrate, as was reported for Junin arenavirus (JUNV) [35] in which the JUNV NP delays the onset of apoptosis by acting as a ‘caspase sink’, diverting caspase-3 from the cleavage of downstream effectors. An equivalent scenario for TULV NP is entirely consistent with our findings that TULV NP associates with casp-3C and is cleaved, as well as the established ability of TULV to delay the apoptotic response.

However, we suggest that NP might delay or hinder the apoptotic response using a different mechanism. The ability of NP to interact with casp-3C, as determined by both indirect

immunofluorescent imaging and immunoprecipitation analysis revelas a highly robust interaction. Interestingly, line scans (Fig 7b) revealed that the TULV NP and casp-3C colocalizing signals were not precisely occupying the same positions, rather NP appeared to form a distinct boundary around casp-3C, suggestive of a virus-induced compartment in which casp-3C was physically separated from the cytosolic environment. The demonstration that casp-3C and NP could be immunoprecipitated by NP antisera is perhaps not surprising given the extensive immunofluorescent colocalization described above, however it reveals a robust and stable casp-3C/NP interaction, and one that differs from a canonical enzyme:substrate interaction that involves binding at the active site alone. The apparent stability of the TULV NP and casp-3C interaction, as demonstrated by their co-immunoprecipitation, argues that the interaction likely encompasses additional residues outside of the active site, and that the association of these two components is not transient.

Based on this evidence, we propose a model in which TULV NP compartmentalizes casp-3C and physically separates it from downstream components of the caspase apoptotic cascasde. This mechanism of apoptosis protection has been previously demonstrated in other types of human disease. In Alzheimer's disease, amyloid-β (Aβ) fibrils sequester caspase-3 into compartments to protect cells from apoptosis [36]. Heat shock protein 27 (Hsp27) also sequesters procaspase-3 and cytochrome-c which prevents the formation of the apoptosome during thermotolerance [37]. In addition, the ced-9 molecule, a Bcl-2 homolog, found in *Caenorhabditis elegans* is a well-established example of a protein that regulates apoptosis by sequestering the caspase-activating factor ced-4, an analogue of mammalian Apaf-1, to the mitochondria, preventing non-programmed apoptosis. When the interaction between ced-9 and ced-4 is disrupted, downstream caspase cleavage and it subsequent activation result in apoptosis [38–40]. These examples provide precedent for apoptotic protein sequestration acting to prevent apoptosis in both health and disease systems.

In summary, the colocalization and co-precipitation of TULV NP and casp-3C, paired with the presence of a casp-3C recognition site provides evidence that NP is involved in interference of the host cell apoptotic pathway. We therefore suggest that TULV NP interferes with apoptosis by binding to and sequestering active caspase-3 in NP-coated compartments preventing casp-3C activation of its downstream substrates.

Author contributions

Author contributions are as follows: JNB, KD, RH and TAE conceptualized the study; KD performed the experimental investigation; KD and JNB wrote the original draft manuscript; KD, JM, JF and JNB reviewed and edited the manuscript; TAE, JM and JNB supervised the core team; JNB, RH provided management and coordination of the research activities and acquired the financial support for the project.

Conflict of interests

The authors declare that they have no conflicts of interest with the contents of this article

Funding information

This work was funded by a joint University of Leeds Anniversary 110 Scholarship, Public Health England (PHE) PhD studentship to KD and PHE studentship to JF

References

1. **Schmaljohn CS, Dalrymple JM**. Analysis of Hantaan virus RNA: evidence for a new genus of bunyaviridae. *Virology* 1983;131:482–91.
2. **Schmaljohn CS, Hasty SE, Harrison SA, Dalrymple JM**. Characterization of hantaan virions, the prototype virus of hemorrhagic fever with renal syndrome. *J Infect Dis* 1983;148:1005–1012.
3. **Plyusnin A**. Genetics of hantaviruses: implications to taxonomy. *Arch Virol* 2002;147:665–82.
4. **Virtanen JO, Jääskeläinen KM, Djupsjöbacka J, Vaheri A, Plyusnin A, *et al.*** Tula hantavirus NSs protein accumulates in the perinuclear area in infected and transfected cells. *Arch Virol* 2010;155:117–121.
5. **Matthys V, Mackow ER**. Hantavirus Regulation of Type I Interferon Responses. *Adv Virol* 2012;2012:1–9.
6. **Briese T, Alkhovsky S V., Beer M, Calisher CH, Charrel RN, *et al.*** Bunyavirales proposal. *Ictv* 2016;1–45.
7. **Guo W-PP, Lin X-DD, Wang W, Tian J-HH, Cong M-LL, *et al.*** Phylogeny and Origins of Hantaviruses Harbored by Bats, Insectivores, and Rodents. *PLoS Pathog* 2013;9:e1003159.
8. **Shi M, Lin X-D, Chen X, Tian J-H, Chen L-J, *et al.*** The evolutionary history of vertebrate RNA viruses. *Nature* 2018;556:197–202.
9. **Plyusnin A, Morzunov SP**. Virus Evolution and Genetic Diversity of Hantaviruses and Their Rodent Hosts. Springer, Berlin, Heidelberg. pp. 47–75.
10. **Rowe JE, Wagoner K, Jentes ES, Root JJ, Beaty BJ, *et al.*** Epizootiology of Sin Nombre and El Moro Canyon Hantavirus, Southeastern Colorado, 1995-2000. *J Wildl Dis* 2013;41:1–11.
11. **Kallio ER, Voutilainen L, Vapalahti O, Vaheri A, Henttonen H, *et al.*** Endemic hantavirus infection impairs the winter survival of its rodent host. *Ecology* 2007;88:1911–6.
12. **Kallio ER, Klingström J, Gustafsson E, Manni T, Vaheri A, *et al.*** Prolonged survival of Puumala hantavirus outside the host: Evidence for indirect transmission via the environment. *J Gen Virol* 2006;87:2127–2134.
13. **Botten J, Mirowsky K, Kusewitt D, Ye C, Gottlieb K, *et al.*** Persistent Sin Nombre Virus Infection in the Deer Mouse (Peromyscus maniculatus) Model: Sites of Replication and Strand-Specific Expression. *J Virol* 2003;77:1540–1550.
14. **Miedema K, Schountz T, McGuire A, Fauver J, Rico A, *et al.*** Maporal Hantavirus Causes Mild Pathology in Deer Mice (Peromyscus maniculatus). *Viruses* 2016;8:286.
15. **Martinez-Valdebenito C, Calvo M, Vial C, Mansilla R, Marco C, *et al.*** Person-to-

person household and nosocomial transmission of andes hantavirus, Southern Chile, 2011. *Emerg Infect Dis* 2014;20:1629–1636.

16. **Brummer-Korvenkontio M, Vaheri A, Hovi T, von Bonsdorff CH, Vuorimies J, *et al.*** Nephropathia epidemica: detection of antigen in bank voles and serologic diagnosis of human infection. *J Infect Dis* 1980;141:131–134.
17. **Feldmann H, Sanchez A, Morzunov S, Spiropoulou CF, Rollin PE, *et al.*** Utilization of autopsy RNA for the synthesis of the nucleocapsid antigen of a newly recognized virus associated with hantavirus pulmonary syndrome. *Virus Res* 1993;30:351–367.
18. **Cosgriff TM**. Mechanisms of Disease in Hantavirus Infection: Pathophysiology of Hemorrhagic Fever with Renal Syndrome. *Clin Infect Dis* 1991;13:97–107.
19. **Meyer BJ, Schmaljohn CS**. Persistent hantavirus infections: characteristics and mechanisms. *Trends Microbiol* 2000;8:61–67.
20. **Vapalahti O, Lundkvist A, Kukkonen SKJ, Cheng Y, Gilljam M, *et al.*** Isolation and characterization of Tula virus, a distinct serotype in the genus Hantavirus, family Bunyaviridae. *J Gen Virol* 1996;77:3063–3067.
21. **Jääskeläinen KM, Plyusnina A, Lundkvist Å, Vaheri A, Plyusnin A**. Tula hantavirus isolate with the full-length ORF for nonstructural protein NSs survives for more consequent passages in interferon-competent cells than the isolate having truncated NSs ORF. *Virol J* 2008;5:3.
22. **Elmore S**. Apoptosis: A Review of Programmed Cell Death. *Toxicol Pathol* 2007;35:495–516.
23. **Li X-DD, Mäkelä TP, Guo D, Soliymani R, Koistinen V, *et al.*** Hantavirus nucleocapsid protein interacts with the Fas-mediated apoptosis enhancer Daxx. *J Gen Virol* 2002;83:759–766.
24. **Park S-W, Han M-G, Park C, Ju YR, Ahn B-Y, *et al.*** Hantaan virus nucleocapsid protein stimulates MDM2-dependent p53 degradation. *J Gen Virol* 2013;94:2424–8.
25. **Solà-Riera C, Gupta S, Ljunggren H-G, Klingström J**. Orthohantaviruses belonging to three phylogroups all inhibit apoptosis in infected target cells. *Sci Rep* 2019;9:834.
26. **Gupta S, Braun M, Tischler ND, Stoltz M, Sundström KB, *et al.*** Hantavirus-infection Confers Resistance to Cytotoxic Lymphocyte-Mediated Apoptosis. *PLoS Pathog*;9. Epub ahead of print 2013. DOI: 10.1371/journal.ppat.1003272.
27. **Kramski M, Meisel H, Klempa B, Krüger DH, Pauli G, *et al.*** Detection and typing of human pathogenic hantaviruses by real-time reverse transcription-PCR and pyrosequencing. *Clin Chem* 2007;53:1899–1905.
28. **McElroy A., Smith J., Hooper J., Schmaljohn C.** Andes virus M genome segment is not sufficient to confer the virulence associated with Andes virus in Syrian hamsters. *Virology* 2004;326:130–139.

29. **Ontiveros SJ, Li Q, Jonsson CB**. Modulation of apoptosis and immune signaling pathways by the Hantaan virus nucleocapsid protein. *Virology* 2010;401:165–178.
30. **Li X-D, Lankinen H, Putkuri N, Vapalahti O, Vaheri A**. Tula hantavirus triggers pro-apoptotic signals of ER stress in Vero E6 cells. *Virology* 2005;333:180–189.
31. **Markotic A, Hensley L, Geisbert T, Spik K, Schmaljohn C**. Hantaviruses induce cytopathic effects and apoptosis in continuous human embryonic kidney cells. *J Gen Virol* 2003;84:2197–2202.
32. **Li X-DX-D, Kukkonen S, Vapalahti O, Plyusnin A, Lankinen H, *et al.*** Tula hantavirus infection of Vero E6 cells induces apoptosis involving caspase 8 activation. *J Gen Virol* 2004;85:3261–3268.
33. **Garg H, Mohl J, Joshi A**. HIV-1 induced bystander apoptosis. *Viruses* 2012;4:3020–43.
34. **Karjoo Z, Chen X, Hatefi A**. Progress and problems with the use of suicide genes for targeted cancer therapy. *Adv Drug Deliv Rev* 2016;99:113–128.
35. **Wolff S, Becker S, Groseth A**. Cleavage of the Junin Virus Nucleoprotein Serves a Decoy Function To Inhibit the Induction of Apoptosis during Infection. *J Virol* 2013;87:224–233.
36. **Chang Y-J, Linh NH, Shih YH, Yu H-M, Li MS, *et al.*** Alzheimer's Amyloid-β Sequesters Caspase-3 in Vitro via Its C-Terminal Tail. *ACS Chem Neurosci* 2016;7:1097–1106.
37. **Concannon CG, Orrenius S, Samali A**. Hsp27 inhibits cytochrome c-mediated caspase activation by sequestering both pro-caspase-3 and cytochrome c. *Gene Expr* 2001;9:195–201.
38. **Hengartner MO, Ellis R, Horvitz R**. Caenorhabditis elegans gene ced-9 protects cells from programmed cell death. *Nature* 1992;356:494–499.
39. **Yan N, Chai J, Lee ES, Gu L, Liu Q, *et al.*** Structure of the CED-4–CED-9 complex provides insights into programmed cell death in Caenorhabditis elegans. *Nature* 2005;437:831–837.
40. **Tan FJ, Fire AZ, Hill RB**. Regulation of apoptosis by C. elegans CED-9 in the absence of the C-terminal transmembrane domain. *Cell Death Differ* 2007;14:1925–35.

Figure legends

Figure 1. Identification and quantification of TULV components. a) Bacterially expressed and purified recombinant SEOV NP_{core} used for antigen production migrated with an apparent molecular weight of ~30 kDa following SDS-PAGE, as visualized by Coomassie staining. The SEOV NP_{core} was detected using NP_{core} antisera by western blotting. b) Cross-reactivity of the SEOV NP_{core} antisera against TULV NP (~50 kDa) expressed in infected Vero E6 cell lysates, shown by western blotting. Cell lysates were collected at 120 hpi and GAPDH used as a loading control. c) Indirect immunofluorescence images of TULV infected and mock infected Vero E6 cells using the NP antisera, taken on a Zeiss LSM880 confocal microscope using x40 magnification, with the white bar representing 20 µM. Nuclei are shown in blue and TULV NP is shown in green. d) *In vitro* transcribed TULV S segment vRNA, serially diluted to form a calibration curve for quantitative RT-PCR. e) Example calibration curve generated experimentally by quantitative RT-PCR.

Figure 2. TULV Immunofluorescent infectivity assay. a) An example of a neutral red plaque assay well at 10^{-3} dilution displaying typical indistinct hantavirus plaques. b) Example images of TULV-infected or mock-infected wells used for the immunofluorescent infectivity assay using anti-NP antisera and the Incucyte ZOOM instrument, with (IF) and without (object mask) analysis using masking software to count immunofluorescent units. c) Linear range describing dilution factor of immunofluorescent assay.

Figure 3. Kinetics of TULV replication in Vero E6 cells. a) Western blot using anti-TULV NP and anti-GAPDH antibodies of TULV-infected Vero E6 cell lysates collected at time points spanning 1-10 dpi, with NP levels quantified using densitometry in relation to the GAPDH loading control. b) TULV RNA genome copies per ml as quantified using one-step quantitative RT-PCR on samples collected 1-10 dpi, and c) extended to 1-30 dpi. d) TULV infectious titres determined by the immunofluorescence infectivity assay on samples collected 1-10 dpi, and e) extended to 1-30 dpi. f) Laser scanning confocal images taken of TULV infected Vero E6 cells at 1.5 dpi, 7 dpi and 30 dpi using 40x magnification stained using anti-TULV NP antisera, with the white bar representing 20 µM. Nuclei were stained with DAPI and shown in blue and TULV NP is shown in green.

Figure 4. Examination of the induction of apoptotic markers during TULV infection of vero E6 cells TULV infected Vero E6 cell lysates collected from 1-10 dpi and 30 dpi and

examined by western blotting for the presence of TULV NP, pre-caspase 3 (casp-3), active caspase 3 (casp-3C) and cleaved PARP (PARP-C) alongside a GAPDH loading control.

Figure 5. Detection of active cleaved caspase 3 in bystander cells, but not infected cells, within TULV infected Vero E6 cultures. a) Indirect immunofluorescence of TULV-infected Vero E6 cells at 1.5 dpi using antisera specific for TULV NP and cleaved caspase 3 (casp-3C). Images were taken using laser scanning confocal microscopy using 40x magnification, with casp-3C shown in red, TULV NP shown in green, and DAPI in blue. The white bar represents 20 µM. b) Merged zoom images of four representative bystander cells with white bar representing 10 µM. c). Quantification of the percentage of TULV-infected and bystander cells exhibiting casp-3C staining. d). Fluorescent line scans of both bystander and TULV infected cells of the right hand merge panel shown in panel a, taken along grey bars using Fiji software, with the red line representing NP and green line representing casp-3C .

Figure 6. Active caspase 3 colocalises with TULV NP in the cytoplasm at later stages of infection. a) Indirect immunofluorescence of Vero E6 cells infected with TULV at 7 dpi, or b) 30 dpi. Images taken using laser scanning confocal microscopy using 100x magnification, with casp-3C signal in red, nucleocapsid protein (NP) in green and DAPI in blue, with the white bar representing 20 µM. Merged images are shown on the right, with a zoomed merge in which the white bar represents 10 µM. A fluorescent line scan was taken along the grey the bar shown on the zoomed merged image using Fiji software, with the red line representing NP and green line representing casp-3C.

Figure 7. Widefield deconvolution microscopy suggests TULV NP sequesters active caspase 3 within compartments. a) Indirect immunofluorescence of Vero E6 cells persistently infected with TULV at 30 dpi. Images taken using widefield deconvolution microscopy using 100x magnification, with casp-3C signal in red, nucleocapsid protein (NP) in green and DAPI in blue. Dashed boxes delineates inset, white bar represents 20 µM b) Zoomed images of inset b shown in panel a, with individual and merged channels shown, with white bar representing 10µM and position of three fluorescent line scans shown as grey bars, taken using Fiji software. Green line represents NP and red line signal indicates casp-3C. Histogram displays percentage of NP puncta or structures which display colocalisating signals for TULV NP and casp-3C. For each time point (1.5 dpi, 7 dpi, 30 dpi) 100 puncta/structures were counted using Fiji software. c) Fluorescent line scans taken using Fiji software of regions of discrete casp-3C staining within inset c shown in panel a and plotted with the green line representing NP and the red line representing casp-3C.

Figure 8. TULV NP possesses a caspase-3 cleavage site and is cleaved during apoptosis a) Multiple sequence alignment of TULV, SEOV, HTNV, PHV and ANDV NP protein sequences carried out in Clustal W and analysed using Jalview software. The red box highlights the identified caspase-3 cleavage sites b) TULV NP cell lysates examined for the presecence of TULV NP (FL NP) and the cleavage products at 32 kDa and 16 kDa. c) Immunoprecipitation using TULV NP antisera coprecipitates full-length and cleaved forms of TULV NP (50 kDa) along with casp 3-C (17 kDa)

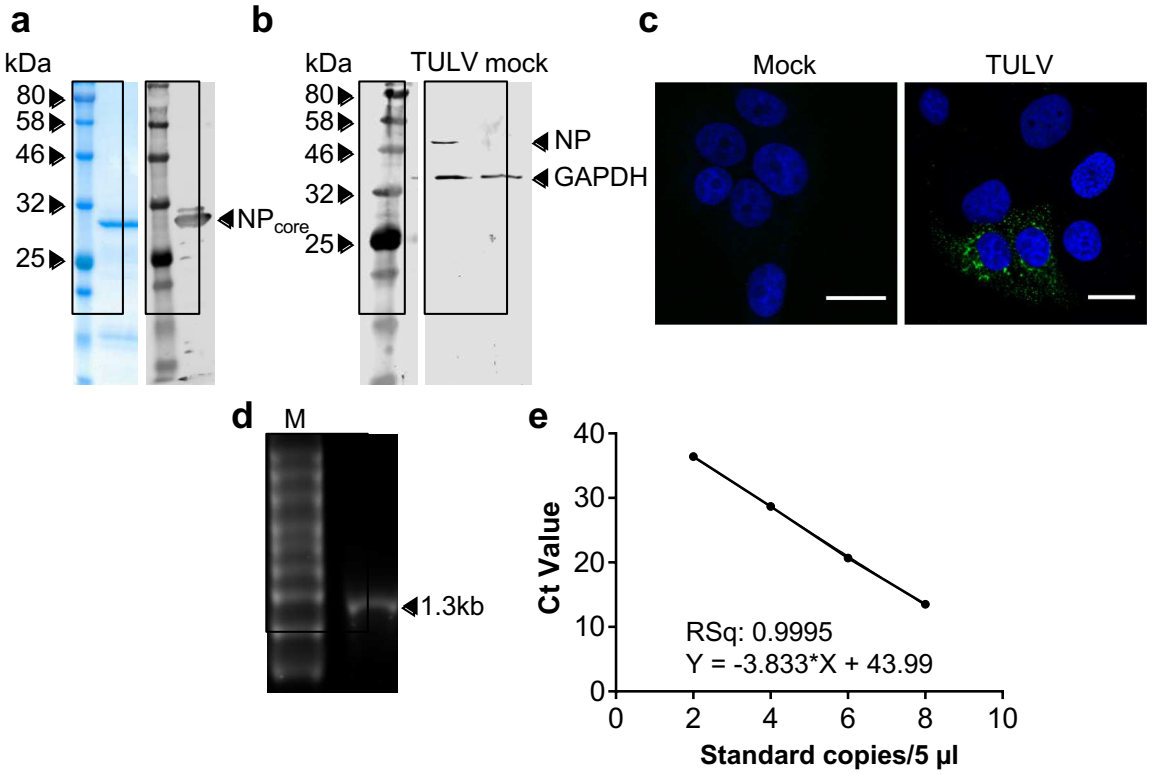
a
kDa
80
58
46
32
25
NP core
b
kDa
TULV mock
80
58
46
32
25
NP
GAPDH
c
Mock
TULV
d
M
1.3kb
e
Ct Value
40
30
20
10
0
0
2
4
6
8
10
RSq: 0.9995
Y = -3.833*X + 43.99
Standard copies/5 µl

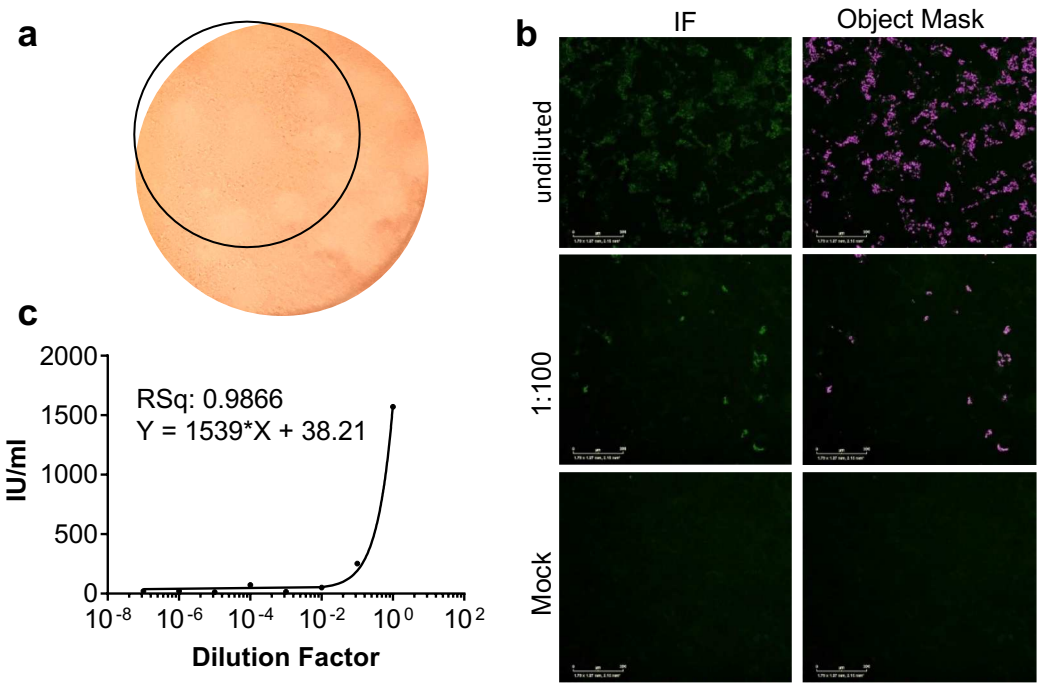
a
b
IF
Object Mask
undiluted
1:100
Mock
c
2000
1500
1000
500
0
IU/ml
RSq: 0.9866
Y = 1539*X + 38.21
10-8
10-6
10-4
10-2
100
102
Dilution Factor

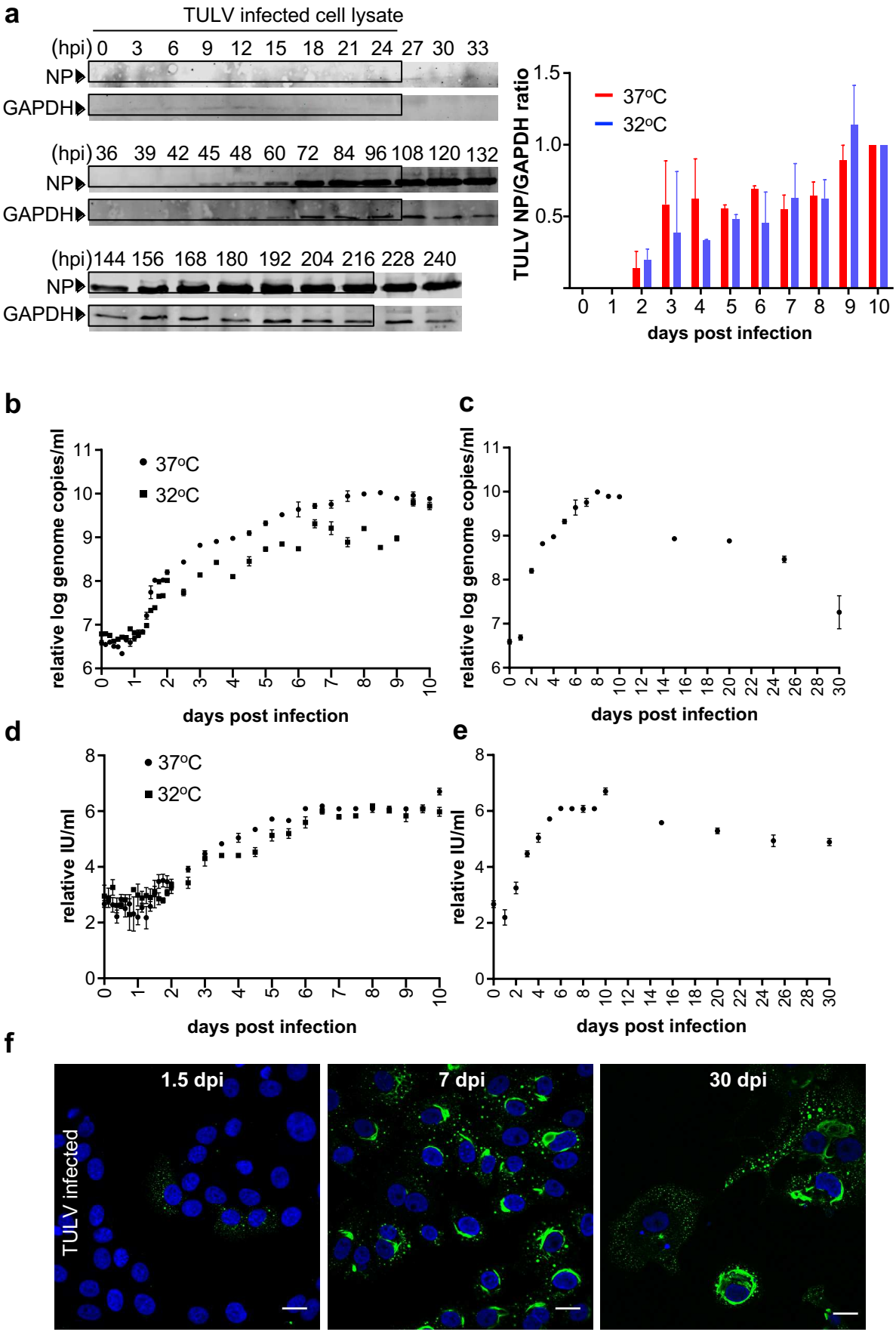
a
TULV infected cell lysate
(hpi) 0 3 6 9 12 15 18 21 24 27 30 33
NP
GAPDH
(hpi) 36 39 42 45 48 60 72 84 96 108 120 132
NP
GAPDH
(hpi) 144 156 168 180 192 204 216 228 240
NP
GAPDH
TULV NP/GAPDH ratio
37°C
32°C
days post infection
b
relative log genome copies/ml
37°C
32°C
days post infection
c
relative log genome copies/ml
days post infection
d
relative IU/ml
37°C
32°C
days post infection
e
relative IU/ml
days post infection
f
1.5 dpi
7 dpi
30 dpi
TULV infected

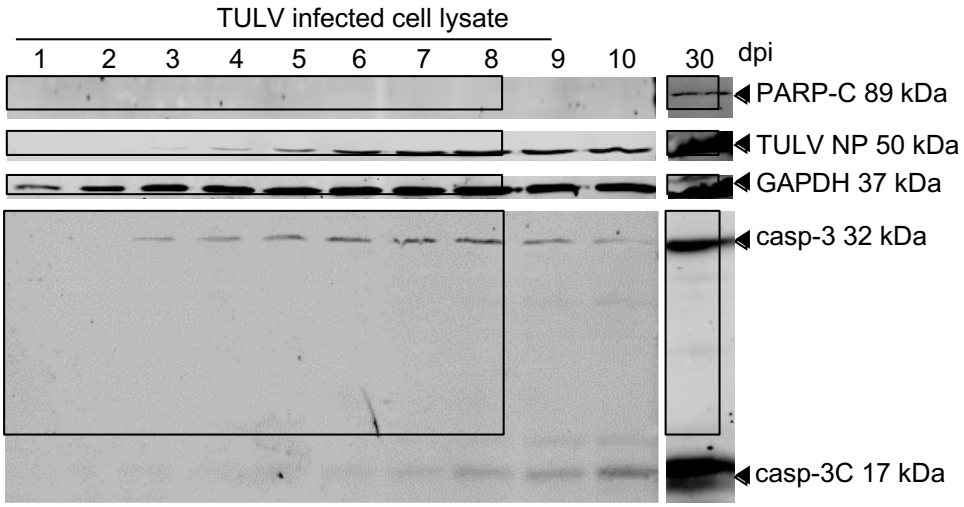
TULV infected cell lysate
1
2
3
4
5
6
7
8
9
10
30
dpi
PARP-C 89 kDa
TULV NP 50 kDa
GAPDH 37 kDa
casp-3 32 kDa
casp-3C 17 kDa

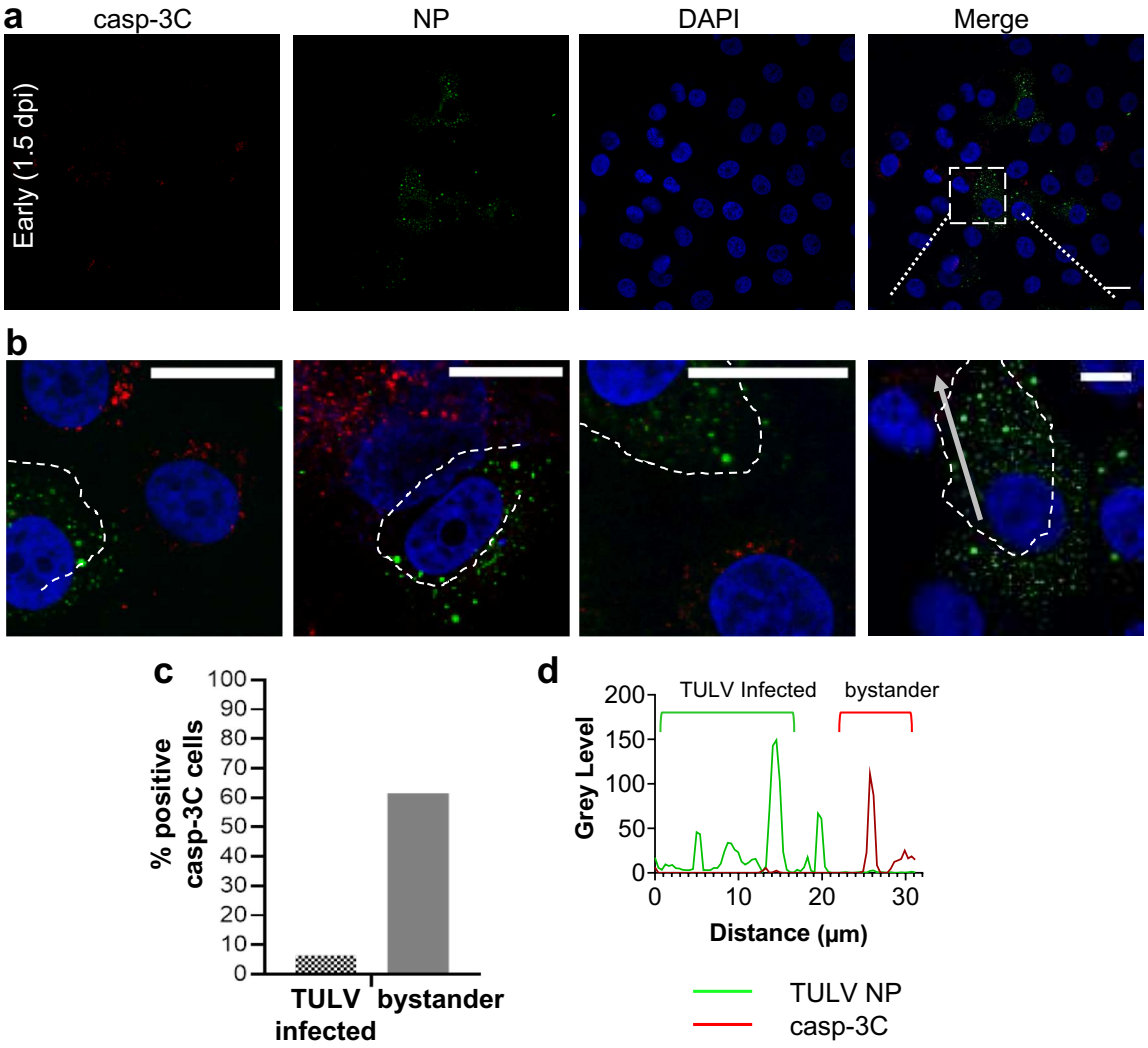
a
casp-3C
NP
DAPI
Merge
Early (1.5 dpi)
b
c
% positive casp-3C cells
100
90
80
70
60
50
40
30
20
10
0
TULV infected
bystander
d
TULV Infected
bystander
Grey Level
200
150
100
50
0
0
10
20
30
Distance (µm)
TULV NP
casp-3C

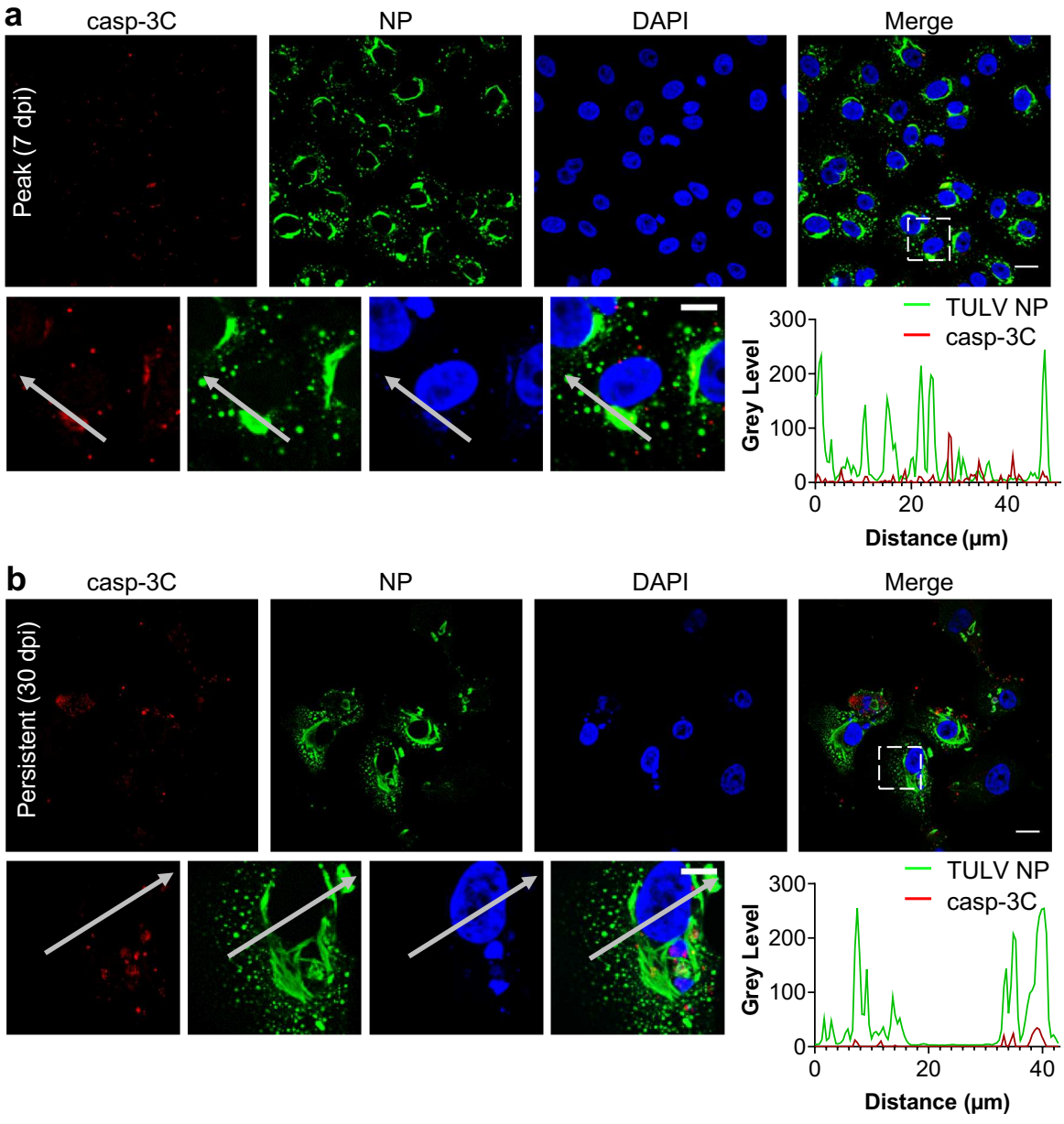
a
casp-3C
NP
DAPI
Merge
Peak (7 dpi)
TULV NP
casp-3C
Grey Level
300
200
100
0
0
20
40
Distance (µm)
b
casp-3C
NP
DAPI
Merge
Persistent (30 dpi)
TULV NP
casp-3C
Grey Level
300
200
100
0
0
20
40
Distance (µm)

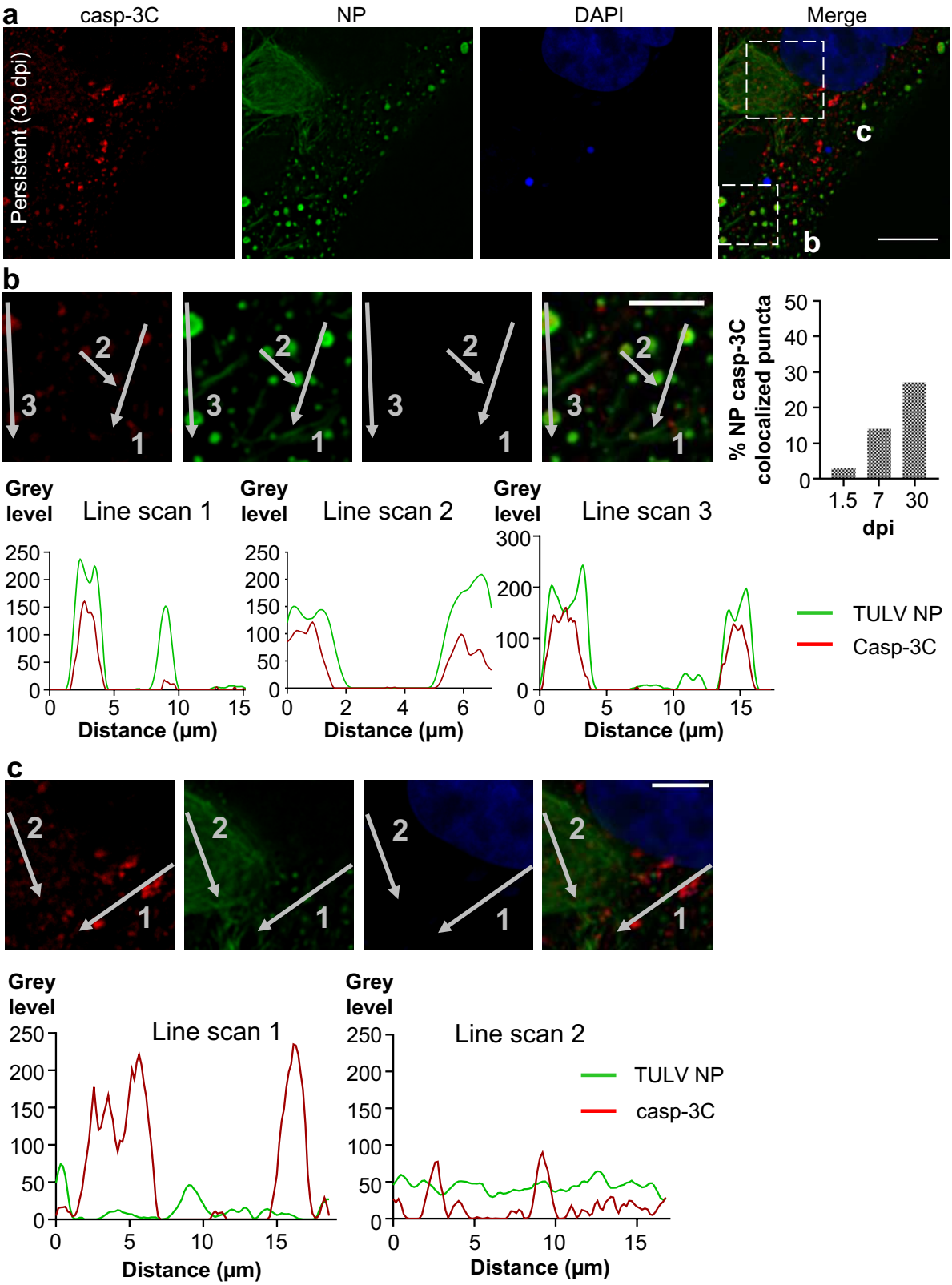
a
casp-3C
NP
DAPI
Merge
Persistent (30 dpi)
c
b
b
2
3
1
% NP casp-3C colocalized puncta
50
40
30
20
10
0
1.5
7
30
dpi
Grey level
Line scan 1
Line scan 2
Line scan 3
250
200
150
100
50
0
300
0
5
10
15
2
4
6
Distance (μm)
TULV NP
Casp-3C
c
2
1
Grey level
Line scan 1
Line scan 2
TULV NP
casp-3C
Distance (μm)

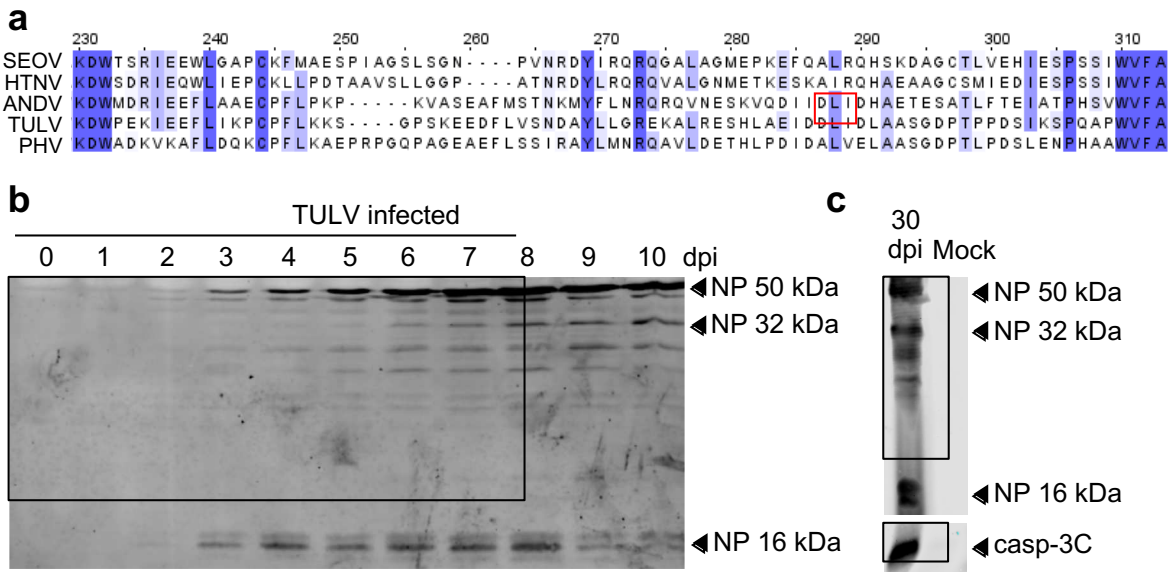
a
230
240
250
260
270
280
290
300
310
SEOV KDWTSRIEEWLGAPCKFMAESPIAGSLSGN----PVNRDYIRQRQGALAGMEPKEFQALRQHSKDAGCTLVEHIESPSSIWVFA
HTNV KDWSDRIEQWLIEPCKLLPDTAAVSLLGGP----ATNRDYLRQRQVALGNMETKESKAIRQHAEAAGCSMIEDIESPSSIWVFA
ANDV KDWMDRIEEFLAAECPFLPKP-----KVASEAFMSTNKMYFLNRQRQVNESKVQDIIDLIDHAETESATLFTEIATPHSVWVFA
TULV KDWPEKIEEFLIKPCPFLKKS----GPSKEEDFLVSNDAYLLGREKALRESHLAEIDDLIDLAASGDPTPPDSIKSPQAPWVFA
PHV KDWADKVKAFLDQKCPFLKAEPRPGQPAGEAEFLSSIRAYLMNRQAVLDETHLPDIDALVELAASGDPTLPDSLENPHAAWVFA
b
TULV infected
0 1 2 3 4 5 6 7 8 9 10 dpi
NP 50 kDa
NP 32 kDa
NP 16 kDa
c
30 dpi Mock
NP 50 kDa
NP 32 kDa
NP 16 kDa
casp-3C